JPE 17-4-11

https://doi.org/10.6113/JPE.2017.17.4.953
ISSN(Print): 1598-2092 / ISSN(Online): 2093-4718

Precise Braking Torque Control for Momentum Flywheels Based on a Singular Perturbation Analysis

Xinxiu Zhou* and Dan Su†

*School of Instrument Science and Optoelectronic Engineering, Beihang University, Beijing, China
†Department of Mechanical and Biomedical Engineering, City University of Hong Kong, Hong Kong SAR, China

Abstract

Momentum flywheels are widely applied for the generation of small and precise torque for the attitude control and inertial stabilization of satellites and space stations. Due to its inherited system nonlinearity, the tracking performance of the flywheel torque/speed in dynamic/plug braking operations is limited when a conventional controller is employed. To take advantage of the well-separated two-time-scale quantities of a flywheel driving system, the singular perturbation technique is adopted to improve the torque tracking performance. In addition, the composite control law, which combines slow- and fast- dynamic portions, is derived for flywheel driving systems. Furthermore, a novel control strategy for plug braking dynamics, which considers couplings between the Buck converter and the three-phase inverter load, is designed with easy implementation. Finally, experimental results are presented to demonstrate the correctness of the analysis and the superiority of the proposed methods.

Key words: Brushless DC motor, Flywheel rotor, Singular perturbation theory

I. INTRODUCTION

The momentum flywheel is the key actuator for the attitude control of space stations, satellites, etc., [1]-[3]. Traditionally, the torque command of the flywheel periodically changes according to the attitude command of the spacecraft [4]. Meanwhile, the flywheel motor operates alternately between motoring and braking operations to precisely track the reference torque [5]. Therefore, the high-performance controllers designed for braking operations are as important as the one for motoring operation [6], [7]. Typically, there are three kinds of braking methods [5], i.e., regenerative braking, dynamic braking and plug braking. Plug braking and dynamic braking are applied in low-speed and high-speed ranges, respectively, while regenerative braking is rarely used in attitude control flywheel driving systems because the dc/dc converter or ultracapacitor, which is responsible for obtaining the regenerative energy [8], will results in increased complexity of the controller design and hardware configurations as well as a decrease in the system reliability.

Manuscript received Sep. 30, 2016; accepted Mar. 6, 2017
Recommended for publication by Associate Editor Dong-Hee Lee.
†Corresponding Author: dansu7-c@my.cityu.edu.hk
Tel: +852-34426778, City University of Hong Kong
*School of Instrument Science and Optoelectronic Engineering, Beihang University, China

During the past few decades, a majority of the publications on motor driving systems have focused on motoring operation. Due to the development of hybrid electric vehicles (HEVs) [9]-[11] and smart power grids [12], regenerative braking has also attracted an increasing amount of attention. However, motoring operation possesses better linearity than braking operation and regenerative braking, which usually evaluate the high regenerative efficiency [13] that does not demand high-precision torque/speed tracking performance. Therefore, the control methods used in motoring operation and regenerative braking cannot be directly applied in the dynamic and plug braking process. At the same time, analytical studies on dynamic and plug braking have been very limited. A flywheel braking torque ripple suppression method was proposed in [5], in which the dynamic braking torque ripple is suppressed by a predictive controller and the plug braking torque ripple is reduced by changing the PWM modulation pattern. However, the proposed predictive controller in [5] does not guarantee decent robustness against system parameter perturbations and the system dynamics in plug braking operation are not fully analyzed. Therefore, further studies are necessary to achieve satisfactory flywheel control performance.

Compared with the other brushless DC motors (BLDCMs) in industrial applications, the two-time-scale quantities of the BLDCMs in flywheels are better separated for two reasons.

© 2017 KIPE

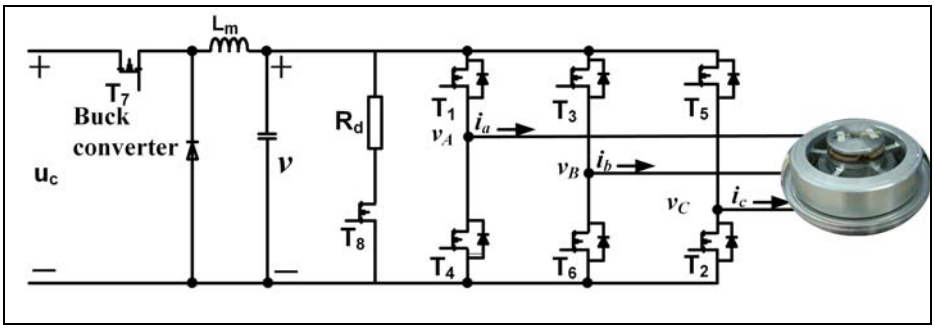

Fig. 1. Buck converter-based BLDCM drive system block.

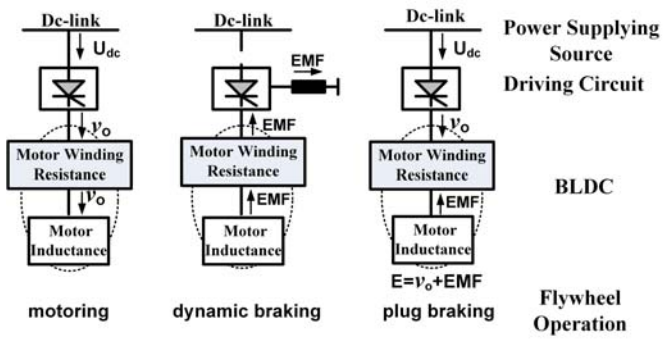

Fig. 2. Energy flow diagrams.

First, permanent magnet motors with a coreless stator are usually used in flywheel driving systems in the aerospace application owing to the absence of core loss [7], [14], which leads to a small motor inductance. Second, flywheels have a larger inertial moment than slender rod driving motors. It is widely accepted that the singular perturbation technique serves as an effective tool to deal with multiple-time-scale linear and nonlinear systems [15], [16]. Therefore, it is well-suited for analyzing flywheel driving systems. Meanwhile, the singular perturbation technique can provide us more insights into the dynamic couplings in plug braking dynamics, which the traditional distributed PID regulator fails to consider. Based on the singular perturbation analysis, the variable structure controller [20], [21] is adopted in this paper to achieve high-precision torque/speed tracking performance with easy implementation.

This paper is organized as follows. Section II describes the model of dynamic braking and proposes a composite controller design strategy which combines slow- and fast- time portions based on the singular perturbation theory. Meanwhile, a simple control strategy for plug braking is proposed in Section III. Discussions of the main experimental results are presented in Section IV. Finally, some conclusions are stated in Section V.

II. Modelling and Composite Controller Design for Dynamic Braking

Fig. 1 and Fig. 2 show the configuration of a flywheel motor driving system [18] and the energy flow in three different operations, respectively. In the motoring process, the electrical energy provided by a DC power source is transformed into the kinematic energy stored by a flywheel and thermal energy dissipated by the driving circuit. In the dynamic braking operation, kinematic energy is converted into thermal energy on the dynamic braking resistance to generate braking torque. When the rotation velocity of the flywheel is below a certain level, the back electromotive is insufficient to generate torque with required magnitude. Therefore, the Buck converter is modulated to supply plug braking voltage. Due to the energy limitations in satellites, it is useful to operate the motor first as a generator (dynamic braking) and then as a plug brake (plug braking) to perform the full braking action from running speed to standstill. Clearly, the system dynamics of plug braking is more complex than that of dynamic braking. Therefore, the analysis on dynamic braking is given first.

Before modeling and designing the controller for a momentum flywheel system in braking operation, the singularly perturbed model applied in this paper is briefly introduced here. Consider the following class of singularly perturbed systems having the following form [15]:

$$\begin{cases} \dfrac{dx}{dt} = A_{11}x + A_{12}z & x(t_0) = x_0 \\ \varepsilon \dfrac{dz}{dt} = A_{21}x + A_{22}z + B(z)u & z(t_0) = z_0 \end{cases} \tag{1}$$

where x and z are the slow and fast dynamic states of the system (1), and ε is a small non-negative parameter. By setting $\varepsilon = 0$, the slow-dynamic subsystem obtained from (1) can be described as [23]:

$$\begin{cases} \dfrac{dx}{dt} = A_{11}x + A_{12}z^s \\ 0 = A_{21}x + A_{22}z^s + B(z^s)u^s \end{cases} \tag{2}$$

where the superscript s denotes the Quasi static component of the corresponding state. If the feedback controller law u^s depends on x^s only, there exists a smooth isolated solution for equation (2) with respect to z^s in the form $z^s=h(x^s, u^s(x^s))$. The slow-dynamic subsystem can be re-described as [16]:

$$\begin{cases} \dfrac{dx}{dt} = A_{11}x + A_{12}h(x,u^s(x)) \\ z^s = h(x,u^s(x)) \end{cases} \tag{3}$$

Therefore, the first step of the controller design for (1) is to look for a control law $u^s(x^s)$ to guarantee the closed-loop stability of the Quasi static component of the state variables in (3). Meanwhile, in order to maintain the validity of the control structure designed for (3), a control law that limits the effect of the boundary layer component of (1) on the system states x and z^s should be synthesized. To this end, consider the reduced fast subsystem as [23]:

$$\varepsilon\frac{dz^e}{dt} = A_{22}z^e + B(z^s + z^e)u^e \tag{4}$$

where $z^e = z - z^s$ is the boundary layer component of the fast state variable z, while $u^e = u - u^s$ is the boundary layer component of the control law. Thus the second step is to design a control law u^e depending on z^e that can rapidly drive z^e to near zero so that the slow-dynamic model (3) remains valid.

A. Dynamic Braking Operation Analysis

The main current path during dynamic braking is illustrated in Fig. 3.

Based on the average modeling approach, the full-order dynamic equation of a flywheel motor in dynamic braking operation can be derived as:

$$\begin{cases} L_{ab}\dfrac{di}{dt} = k_e\omega - v - 2v_T - R_{ab}i \\ C_b\dfrac{dv}{dt} = i - \dfrac{v}{R_d + R_s}D_{dy} \\ J\dfrac{d\omega}{dt} = -k_t i - B_d\omega - \tau_{dis} \end{cases} \tag{5}$$

where J and ω denote the inertial moment and angular speed of the flywheel rotor, k_t is the torque coefficient, k_e is the line-to-line back electromotive force (EMF) coefficient, B_d is the velocity damping coefficient, τ_{dis} is the disturbance torque, i is the motor winding current, v is the Buck converter terminal voltage, v_T is the diode conduction voltage, R_{ab} is the line-winding resistance, C_b is the Buck converter parallel capacitance, R_d is the dynamic braking resistance, R_s is the switch conduction resistance, and D_{dy} is the cycle duty ratio of T_8, respectively. In addition, in the following passage, the superscripts s and e denote the quasi steady and boundary layer components of the fast dynamic states, and the subscripts dy, pl and mt represent the control variables in the dynamic braking, plug braking and motoring operations, respectively.

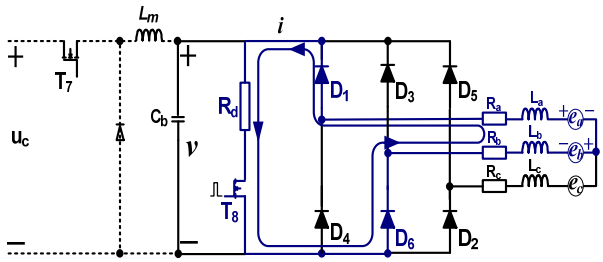

Fig. 3. The main dynamic braking state current path.

Note that L_{ab} and C_b are much smaller than J. Hence, i and v are treated as fast-time states and ω is the slow-time state. According to the singularly perturbed system theory, the slow dynamic subsystem of (5) can be written as:

$$J\frac{d\omega}{dt} = -k_t i^s - B_d\omega - \tau_{dis} \tag{6}$$

$$\begin{cases} 0 = k_e\omega - v^s - 2v_T - R_{ab}i^s \\ 0 = i^s - \dfrac{v^s}{R_d + R_s}D^s_{dy} \end{cases} \tag{7}$$

where D^s_{dy} is the Quasi static component of the control effort.

From (7), the Quasi static components of i^s and v^s can be resolved as:

$$\begin{cases} i^s = f_{dy}(\omega, D^s_{dy}) = \dfrac{k_e\omega - 2v_T}{R_{ab} + (R_d + R_s)/D^s_{dy}} \\ v^s = \dfrac{(k_e\omega - 2v_T)(R_d + R_s)}{(D^s_{dy}R_{ab} + R_d + R_s)} \end{cases} \tag{8}$$

Based on (8), the nonlinear function mapping i^s into D^s_{dy} is given by:

$$D^s_{dy} = f^{-1}_{dy}(\omega, i^s) = \frac{(R_d + R_s)i^s}{(k_e\omega - 2v_T) - R_{ab}i^s} \tag{9}$$

Note that $f^{-1}_{dy}(\omega, i^s)$ is a function of ω. This is because back EMF ($k_e\omega$) provides the braking supply voltage during dynamic braking.

Subtracting (7) from (5), the fast dynamic subsystem is given by:

$$\begin{cases} L_{ab}\dfrac{di^e}{dt} = -R_{ab}i^e - v^e \\ C_b\dfrac{dv^e}{dt} = i^e - \dfrac{D^s_{dy}v^e}{R_d + R_s} - \dfrac{v^s d^e_{dy}}{R_d + R_s} - \dfrac{v^e d^e_{dy}}{R_d + R_s} \end{cases} \tag{10}$$

By applying the small signal modelling technique, the fast dynamic subsystem (10) can be further linearized as:

$$\begin{cases} L_{ab}\dfrac{di^e}{dt} = -R_{ab}i^e - v^e \\ C_b\dfrac{dv^e}{dt} = i^e - \dfrac{D^s_{dy}v^e}{R_d + R_s} - \dfrac{v^s d^e_{dy}}{R_d + R_s} \end{cases} \tag{11}$$

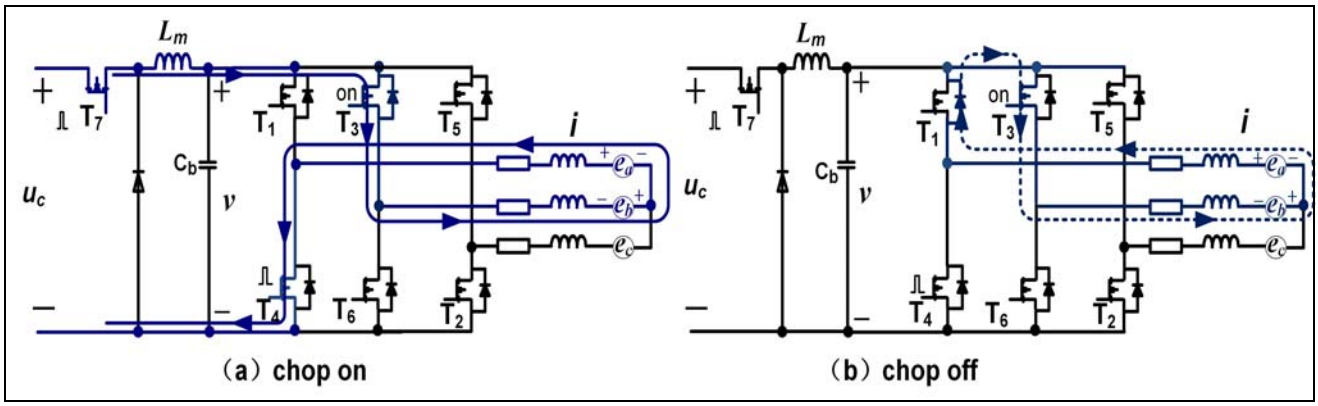

Fig. 4. Plug braking current paths with the ON_PWM pattern.

where $[i^e \quad v^e]=[i \quad v]-[i^s \quad v^s]$ is the boundary layer component of the fast dynamic states, d^e_{dy} is the control law for the fast dynamic subsystem, and the final control effort is a linear combination of the control laws designed for the fast- and slow- dynamic sub-systems, i.e., $d^e+D^s=D$.

B. Dynamic Braking Operation Control Strategy

According to the fast-dynamic and slow-dynamic subsystems given by (6), (7) and (11), the two-time scale controller outputs, i.e., d^e_{dy} and D^s_{dy}, are derived in this part.

When only considering the slow-dynamic subsystem modeled by (6) and (8), the following is obtained:

$$J\frac{d\omega_e}{dt}=-k_t f_{dy}(\omega,D^s)-J\frac{d\omega_r}{dt}-B_d\omega-\tau_{dis} \tag{12}$$

where ω_r denotes the reference speed and $\omega_e=\omega-\omega_r$.

Here the expected speed error differential equation is expected as

$$\gamma_2\int_t\omega_e+\gamma_1\omega_e+\dot{\omega}_e=0 \tag{13}$$

where γ_2 and γ_1 are constant coefficients and $\gamma_2,\gamma_1>0$.

Substituting (13) into (12), the expected slow dynamic system input D^s_{dy} can be obtained as:

$$D^s_{dy}=f^{-1}_{dy}(\omega,\hat{i}^s)=\frac{(R_d+R_s)\hat{i}^s}{(k_e\omega-2v_T)-R_{ab}\hat{i}^s} \tag{14}$$

where $\hat{i}^s=(J\gamma_2\int_t\omega_e+J\gamma_1\omega_e-J\dot{\omega}_r-B_d\omega-\tau_{dis})/k_t$.

Notice that the fast dynamic variables i and v should rapidly converge to the quasi steady components i^s and v^s determined by (8). Upon this, the performance of the slow dynamic subsystem control law (14) can be guaranteed and the influence of the boundary layer components on the slow subsystem can be minimized. Considering that the variable structure control (*VSC*) has the advantages of robustness and easy implementation [22][23], it is applied here to control the boundary layer subsystem.

When the *VSC* switching surface is chosen as $\lambda_{dy}(x^e_{dy})=\lambda^1_{dy}i^e+\lambda^2_{dy}v^e$, the dynamics of (11) on the switching surface can be described as:

$$L_{ab}\frac{di^e}{dt}=-R_{ab}i^e+\lambda^1_{dy}i^e/\lambda^2_{dy} \tag{15}$$

where $\lambda^1_{dy}/\lambda^2_{dy}$ should be smaller than R_{ab} to guarantee system stability. To reduce the computational demand and algorithm complexity, only the variable structure control law in the *VSC* is adopted. Then the variable structure control law can be given by:

$$\begin{aligned}d^e_{dy}&=-(\frac{\partial\lambda_{dy}}{\partial x^e_{dy}}B_e)^{-1}(\sigma\rho_{vs}(\lambda_{dy})+k\lambda_{dy})\\&=\frac{C_b(D^s_{dy}R_{ab}+R_d+R_s)(\sigma\rho_{vs}(\lambda_{dy})+k\lambda_{dy})}{\lambda^2_{dy}(k_e\omega-2v_T)}\end{aligned} \tag{16}$$

where B_e is the input vector of (11), $\rho_{vs}(\lambda_{dy})=f_{lp}(\lambda_{dy}/(|\lambda_{dy}|+\xi))$, $f_{lp}(\ )$ is the low-pass filter operator, and σ and ξ are positive constants. The gain of the variable structure component, i.e. σ, should be large enough to offset uncertainties and matched disturbances [22]. Then the composite control can be obtained as:

$$\begin{aligned}D_{dy}&=D^s_{dy}+d^e_{dy}\\&=f^{-1}_{dy}(\omega,\hat{i}^s)+\frac{C_b(D^s_{dy}R_{ab}+R_d+R_s)(\sigma\rho_{vs}(\lambda_{dy})+k\lambda_{dy})}{\lambda^2_{dy}(k_e\omega-2v_T)}\end{aligned} \tag{17}$$

III. Analysis and Controller Design for Plug Braking

A. Plug Braking Operation Analysis

During plug braking operation, the ON_PWM pattern is applied to reduce the modulation ripple and electromagnetic interference [5]. As illustrated in Fig. 4, the upper switches are used for phase conversion, while the lower switches are employed for regulating the torque current by PWM in the ON_PWM pattern. Meanwhile, the Buck converter is used for offering a plug voltage that is higher than the line-to-line back EMF amplitude to avoid uncontrollable current.

Based on average modeling technology, if the switch conduction resistance R_s is neglected, the differential

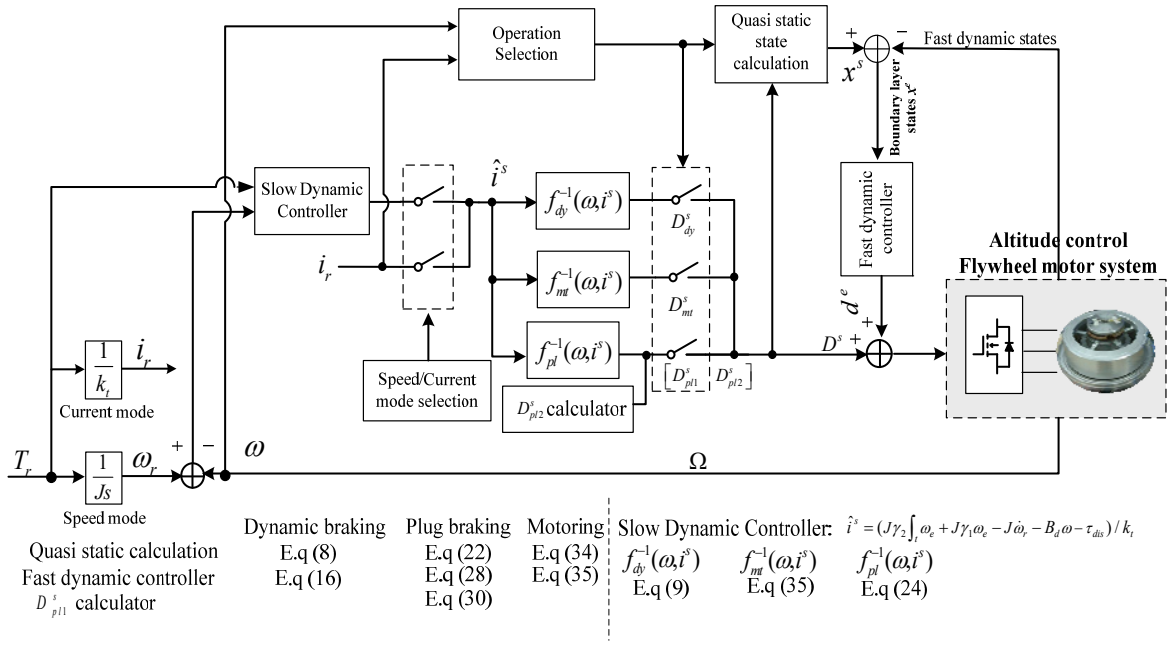

Fig. 5. Overall controller diagram.

equations of the flywheel motor in the plug braking operation can be achieved as:

$$\begin{cases} L_m \dfrac{di_m}{dt} = D_{pl2}(u_c + v_T) - v - v_T \\ L_{ab} \dfrac{di}{dt} = D_{pl1} v + k_e \omega - i R_{ab} - (1 - D_{pl1}) v_T \\ C_b \dfrac{dv}{dt} = (i_m - D_{pl1} i) \\ J\dot{\omega} = -B_d \omega - k_t i - \tau_{dis} \end{cases} \tag{18}$$

where u_c denotes the DC-supply voltage, and D_{pl2} and D_{pl1} are the PWM duty ratios of the switch T_7 and the three-phase inverter (such as T_4 in Fig.4). L_m is the Buck converter inductance, and i_m is the Buck dc-link current. Accordingly, the slow-dynamic subsystem and the fast-dynamic subsystem are described as:

$$\begin{cases} 0 = D^s_{pl2}(u_c + v_T) - v^s - v_T \\ 0 = D^s_{pl1} v^s + k_e \omega - i^s R_{ab} - (1 - D^s_{pl1}) v_T \\ 0 = (i^s_m - D^s_{pl1} i^s) \\ J\dot{\omega} = -B_d \omega - k_t i^s - \tau_{dis} \end{cases} \tag{19}$$

In addition:

$$\begin{cases} L_m \dfrac{di^e_m}{dt} = -v^e + d^e_{pl2}(u_c + v_T) \\ L_{ab} \dfrac{di^e}{dt} = D^s_{pl1} v^e - R_{ab} i^e + (v^s + v_T) d^e_{pl1} + v^s d^e_{pl1} \\ C_b \dfrac{dv^e}{dt} = i^e_m - D^s_{pl1} i^e - i^s d^e_{pl1} - i^e d^e_{pl1} \end{cases} \tag{20}$$

Similarly, the fast dynamic subsystem (20) can be linearized as:

$$\begin{cases} L_m \dfrac{di^e_m}{dt} = -v^e + d^e_{pl2}(u_c + v_T) \\ L_{ab} \dfrac{di^e}{dt} = D^s_{pl1} v^e - R_{ab} i^e + (v^s + v_T) d^e_{pl1} \\ C_b \dfrac{dv^e}{dt} = i^e_m - D^s_{pl1} i^e - i^s d^e_{pl1} \end{cases} \tag{21}$$

From (19), the quasi steady state can be calculated as:

$$\begin{cases} i^s = \hat{f}_{pl}(\omega, D^s_{pl1}, D^s_{pl2}) = (D^s_{pl1} D^s_{pl2}(u_c + v_T) + k_e \omega - v_T) / R_{ab} \\ v^s = D^s_{pl2} u_c - (1 - D^s_{pl2}) v_T \\ i^s_m = D^s_{pl1}(D^s_{pl1} D^s_{pl2}(u_c + v_T) + k_e \omega - v_T) / R_{ab} \end{cases} \tag{22}$$

B. Plug Braking Operation Analysis

A traditional plug braking controller independently regulates Buck output voltage and three-phase inverter current. The basic principle is that the Buck converter regulates the output voltage to reject the influence of the changing load, i.e., BLDCM, and the three-phase inverter is regulated assuming that the supply plug voltage remains constant. However, the couplings of the dynamics of the three-phase inverter and the Buck converter are beyond the consideration of traditional distributed controllers and the controller performance can be improved if these two parts can be analyzed as a whole system. Therefore, a novel control strategy, which analyzes the overall dynamics of plug braking operation, is proposed as follows.

Based on the slow dynamic subsystem described in (19), it can be noted that when a three phase inverter is not ON-PWM modulated, i.e., $D^s_{pl1} = 1$, it follows that $u_{pl} = D^s_{pl2}(u_c+v_T) + k_e\omega - v_T$ can be regarded as the supply voltage to generate the braking torque current i^s through the resistor R_{ab}.

Here u_{pl} is defined as the equivalent plug braking voltage. Since the magnitude of the back EMF $k_e\omega$ declines with respect to the decrease of ω, the equivalent plug braking voltage u_{pl} also decreases with respect to the decline of the rotor speed if D^s_{pl2} remains constant. In order to guarantee that u_{pl} remains at the same level during plug braking operation, the controller law for the Buck duty ratio D^s_{pl2} is designed as $D^s_{pl2}(u_c+v_T)+k_e\omega-v_T=\hat{u}_{pl}$ where $\hat{u}_{pl}$ is a constant. Thus, the following is obtained:

$$D^s_{pl2}=(\hat{u}_{pl}-k_e\omega+v_T)/(u_c+v_T) \tag{23}$$

By substituting (23) into (22), the nonlinear function mapping i^s into D^s_{pl1} can be derived as:

$$D^s_{pl1}=f^{-1}_{pl}(\omega,i^s)=\frac{R_{ab}i^s+v_T-k_e\omega}{\hat{u}_{pl}-k_e\omega+v_T} \tag{24}$$

The controller design process for the slow dynamic subsystem is similar to that of the dynamic braking. Here the expected speed error differential equation is designed as (13). According to (13) and (24), the feedback control design for the slow dynamic subsystem is given by:

$$D^s_{pl1}=f^{-1}_{pl}(\omega,\hat{i}^s)=\frac{R_{ab}\hat{i}^s-k_e\omega+v_T}{\hat{u}_{pl}-k_e\omega+v_T} \tag{25}$$

where $\hat{i}^s=(J\gamma_2\int_t\omega_e+J\gamma_1\omega_e-J\dot{\omega}_r-B_d\omega-\tau_{dis})/k_t$.

From (21), it can be noted that the fast-dynamic subsystem has two inputs d^e_{pl1} and d^e_{pl2}, and that the input vectors for them are $[0\ (v^s+v_T)/L_{ab}\ -i^s/C_b]^{\mathrm{T}}$ and $[(u_c+v_T)/L_m\ 0\ 0]^{\mathrm{T}}$, respectively. The input vector for d^e_{pl2} is independent with the quasi steady states i^s and v^s. Assuming that d^e_{pl2} is selected as a unique input for the system (21), the component $(\partial\lambda_{pl}/\partial x^e_{pl}B_e)^{-1}$ in the variable structure control law is a constant, where $x^e_{pl}=[i^e_m\ i^e\ v^e]^{\mathrm{T}}$ and $\lambda_{pl}(x^e_{pl})=0$ is the designed sliding surface. Therefore, to facilitate the control development, the controller design process is simplified by setting $d^e_{pl1}=0$, and the linearized boundary layer subsystem can be described as:

$$\begin{cases} \dfrac{dz}{dt}=i^e \\ L_m\dfrac{di^e_m}{dt}=-v^e+(u_c+v_T)d^e_{pl2} \\ L_{ab}\dfrac{di^e}{dt}=D^s_{pl1}v^e-R_{ab}i^e \\ C_b\dfrac{dv^e}{dt}=i^e_m-D^s_{pl1}i^e \end{cases} \tag{26}$$

Accordingly, when the sliding surface for the fast dynamic subsystem is chosen as $\lambda_{pl}(i^e,v^e,i^e_{\mathrm{m}})=\lambda^1_{pl}i^e+\lambda^2_{pl}v^e+\lambda^3_{pl}i^e_{\mathrm{m}}$, the dynamic equation on the sliding surface λ_{pl} can be resolved as:

$$\begin{bmatrix} dv^e/dt \\ di^e/dt \end{bmatrix}=\begin{bmatrix} -\lambda^2_{pl}/C_b\lambda^3_{pl} & -\lambda^1_{pl}/C_b\lambda^3_{pl}-D^s_{pl1}/C_b \\ D^s_{pl1}/L_{ab} & -R_{ab}/L_{ab} \end{bmatrix}\begin{bmatrix} v^e \\ i^e \end{bmatrix} \tag{27}$$

The system (27) is exponentially stable as long as $\lambda^2_{pl}/C_b\lambda^3_{pl}+R_{ab}/L_{ab}>0$ and $\lambda^2_{pl}R_{ab}/\lambda^3_{pl}+(D^s_{pl1})^2+\lambda^1_{pl}D^s_{pl1}/\lambda^3_{pl}>0$. If λ^2_{pl} is set as 0, the stability condition can be simplified as $\lambda^1_{pl}/\lambda^3_{pl}>0>-D^s_{pl1}$. Then the control law d^e_{pl2} for the fast dynamic subsystem is obtained as:

$$d^e_{pl2}=-(\frac{\partial\lambda_{pl}}{\partial x^e}B_e)^{-1}(\sigma\rho_{vs}(\lambda_{pl})+k\lambda_{pl})=-\frac{L_m(\sigma\rho_{vs}(\lambda_{pl})+k\lambda_{pl})}{\lambda^3_{pl}(u_c+v_T)} \tag{28}$$

Upon this, the composite control law for the flywheel motor plug braking operation can be derived as:

$$D_{pl2}=D^s_{pl2}+d^e_{pl2}=-\frac{L_m(\sigma\rho_{vs}(\lambda_{pl})+k\lambda_{pl})}{\lambda^3_{pl}(u_c+v_T)}+\frac{(\hat{u}_{pl}-k_e\omega+v_T)}{(u_c+v_T)} \tag{29}$$

$$D_{pl1}=D^s_{pl1}=f^{-1}_{pl}(\omega,\hat{i}^s)=\frac{R_{ab}\hat{i}^s-k_e\omega+v_T}{\hat{u}_{pl}-k_e\omega+v_T} \tag{30}$$

The controller for the motoring operation can be designed by a similar approach, which is illustrated in the Appendix. So far, the composite controller design for a flywheel driving system in the velocity mode is completed. Based on the above analysis, the overall controller diagram is illustrated in Fig. 5, where the top switch in the far left dotted-line block is activated by the velocity/current mode selector.

C. Flywheel Torque Control Strategy Configuration

From the singular perturbation analysis, the functions which map the quasi steady winding current i^s into the duty cycle have been resolved as $f^1_{dy}(\omega,i^s)$, $f^1_{pl}(\omega,i^s)$ and $f^1_{mt}(\omega,i^s)$. In the speed mode controller, the reference torque current, which regulates the rotor speed according to the expected error differential equation (13), is calculated by the slow dynamic controller. Then the *VSC* controller is employed to make the real torque current rapidly converge to the reference torque current. In the current mode controller, the control objective is to regulate the real toque current i to track the reference torque current i^r. Therefore, the only difference between the current mode controller and the speed controller is that the reference quasi steady torque current i^s is the reference torque current in the former one and the slow dynamic controller output in the latter one. Accordingly, the design process for the current mode controller can be described as follows. As shown in Fig.5, when the current mode is selected, the slow dynamic controller does not work and the reference quasi steady torque current i^s is set to be the reference torque current i^r (see Fig.5). Then the quasi steady control component D^s can be achieve from $f^1_{dy}(\omega,i^s)$, and the boundary layer control component d^e can be calculated based on the *VSC* to make the boundary layer component in the fast dynamic states converge to the zero point. Take the dynamic braking operation as an example, the current mode controller can be resolved as:

$$\begin{aligned} D_{dy}&=D^s_{dy}+d^e_{dy} \\ &=f^{-1}_{dy}(\omega,i^r)+\frac{C_b(D^s_{dy}R_{ab}+R_d+R_s)(\sigma\rho_{vs}(\lambda_{dy})+k\lambda_{dy})}{\lambda^2_{dy}(k_e\omega-2v_T)} \end{aligned}$$

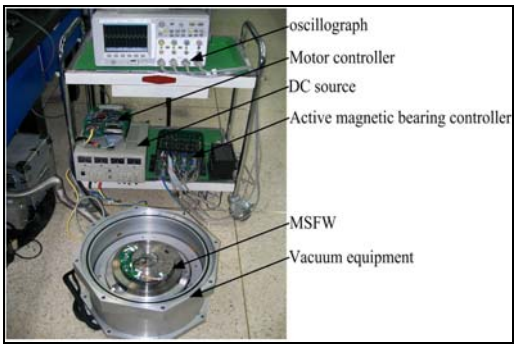

Fig. 6. MSFW control system.

TABLE I
MSFW MOTOR CONTROL SYSTEM PARAMETERS

DC Source	V	28
Rated Output Torque	N·m	±0.05
Rated Rotor Speed	rad/s	±523.6
Moment of Inertia	N·m·s^2/rad	0.0286
Line-to-line Back EMF Cofficient	V·s/rad	0.08
Rated Stator Current	A	2
Phase Resistance	Ω	0.5
Phase Inductance	μH	36
Pole Pairs		6
Buck Converter PWM Frequency	kHz	20

where i^r is the reference torque current.

IV. MSFW MOTOR EXPERIMENTAL RESULTS

A. Experimental Set-up

Fig. 6 illustrates the configuration of the Magnetically Suspended Flywheel (MSFW) control system developed in this study. The validity of the torque control scheme is verified by the BLDCM used in the MSFW for offering torque to adjust the attitude of a satellite. The BLDCM stator is coreless and the back EMF is trapezoidal. The rotor position is measured by means of a 2000-pulse/revolution encoder, and the dc-link current is measured by a high bandwidth Hall effect current sensor. They are then fed into the controller through a 12-bit analog-to-digital (A/D) converter with a 20K Hz sampling frequency. The parameters of the BLDCM control system are listed in Table I. The experimental setup, based on a DSP TMS320C31 and a FPGA EPF10K40 with a 40 MHz oscillator, is implemented.

B. Experiment 1: Torque Mode Flywheel Torque Control

In this experiment, the torque mode control method is verified. Here the torque reference is converted to the current reference according to the equation $T_r=k_t\cdot i_r$. In this mode, the flywheel torque is controlled through directly regulating the phase current. Therefore, the torque mode is known as the current mode as shown in Fig.5. In the experiment, the reference torque is given as T_r= ±0.05N·m, i.e. i_r=0.625A. The system switches from motoring to dynamic braking, and then to plug braking during the whole process. As shown in Fig. 1 and Fig. 3, the dc-link current is equal to the absolute value of the conduction phase current. Therefore, the dc-link current and phase current are sampled at the same time to clearly present the change of the current. In addition, in order to verify the superiority of the proposed method, an experimental comparison between a PID controller and the proposed controller is made as shown in Fig. 7 and Fig. 8. When the flywheel torque controller is designed with a traditional PID algorithm, the electromagnetic torque ($\hat{T}_e=k_t i$) can be controlled to follow the variation of the reference torque during the whole process (see Fig. 7(a)). However, the torque fluctuation is significant during the motoring and braking operations (see Fig. 7(d)-(f)). In addition, when the dynamic braking torque controller is designed with a traditional PID algorithm, the braking torque has a large fluctuation when the system switches from motoring to dynamic braking. Furthermore, the braking torque decreases with the reduction in speed. Notice that the dynamic braking works well in the limited high speed range. When the operating speed is lower than the dynamic braking lower boundary speed value, the required braking torque cannot be held and the dynamic braking is over (see Fig. 7(a)). In addition, from Fig. 7(c), it is found that the actual slope of the rotor speed is lower than the expected value during the motoring process, while it is larger than the expected value during the braking process. This is because there is a difference between the flywheel output torque and the electromagnetic torque under the action of the resistance torque ($T_o=Jd\omega/dt = T_e-\tau_{dis}$).

In order to improve the electromagnetic torque performance, the proposed method is applied to the flywheel system. Through analyzing the slow-time quasi steady state subsystem and the fast-time boundary subsystem in separate time scales, the composite control law is obtained. The waveforms yielded by the proposed controller are shown in Fig. 8. From Fig. 8, it can be found that the torque fluctuation amplitude decreases distinctly during the whole process (see Fig. 8(d)-(f)). It can also be seen that the braking torque is smooth during dynamic braking (see Fig. 8(a)). With the proposed controller the system possesses improved dynamic performance and torque tracking capability.

C. Experiment 2: Speed Mode Flywheel Torque Control

In this experiment the proposed speed mode flywheel torque control scheme is verified. In the speed mode, the speed reference is given as $\omega_r=\int T_r/Jdt$ according to the equation $T_r=J\cdot d\omega_r/dt$. The difference between the torque mode and the speed mode is that they are realized through controlling different variables. The torque mode is realized through controlling the phase current (i.e. electromagnetic torque), while the speed mode is implemented by regulating the change rate of the rotor speed (i.e. the output torque). According to the equation $T_o=J\times d\omega/dt = T_e-\tau_{dis}$, the speed

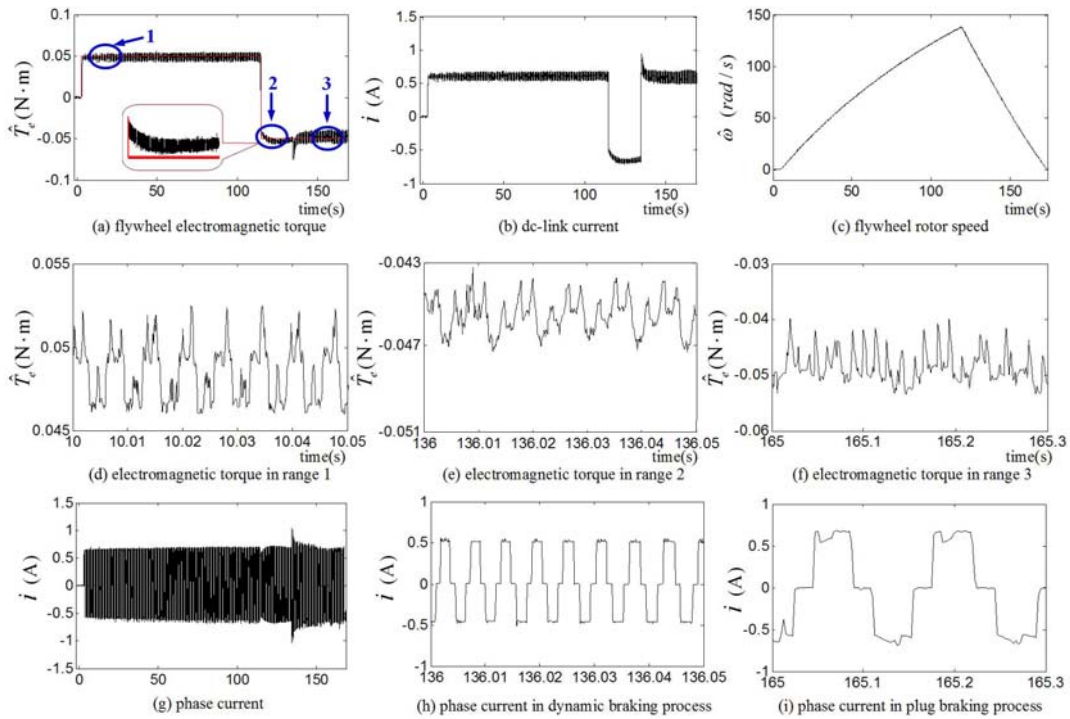

Fig.7. The waveforms yielded by PI controller under torque mode condition.

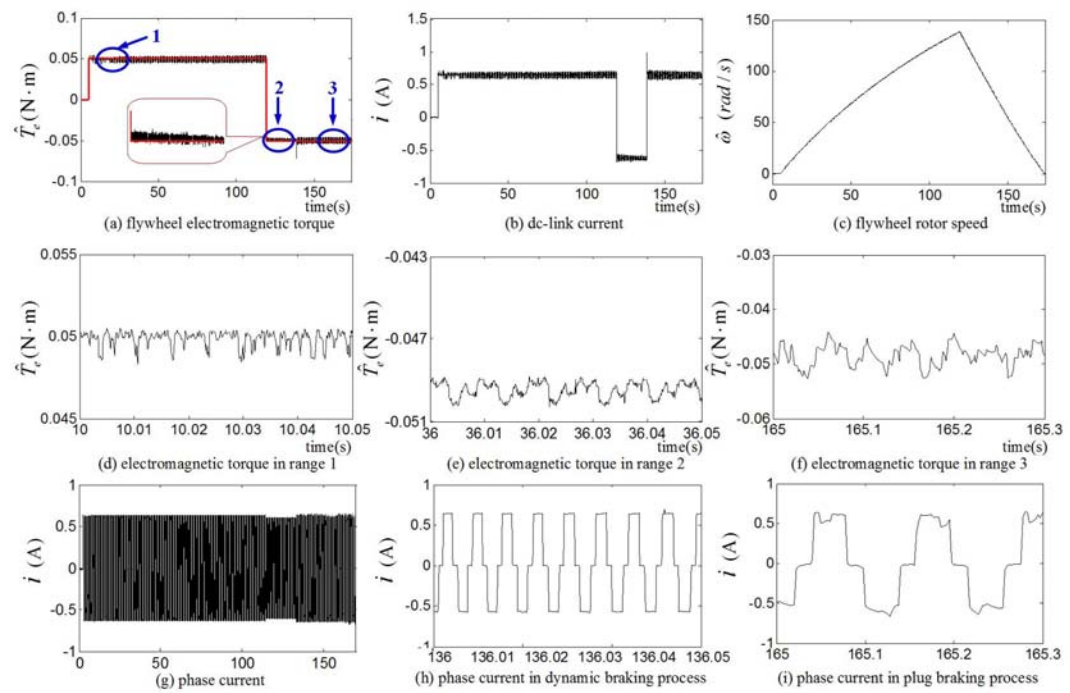

Fig. 8. Waveforms yielded by the proposed controller under the torque mode condition.

mode yields better torque performance due to its disturbance torque suppression ability. In this experiment, reference torque T_r is set to 0.04 N·m (i.e. dω/dt =1.3986rad/s^2), and it changes to -0.05 N·m (dω/dt = - 1.7485rad/s^2) when the rotor speed arrives at 120rad/s. The waveforms yielded by the conventional speed mode torque controller are described in Fig. 9 (I). It can be found that the slope of the rotor speed and the flywheel torque follow the variation of the reference torque during the whole process. However, the speed tracking error is relatively large. The waveforms yielded by the proposed speed mode controller are reported in Fig. 9 (d). It can be seen that the rotor speed and flywheel torque tracking

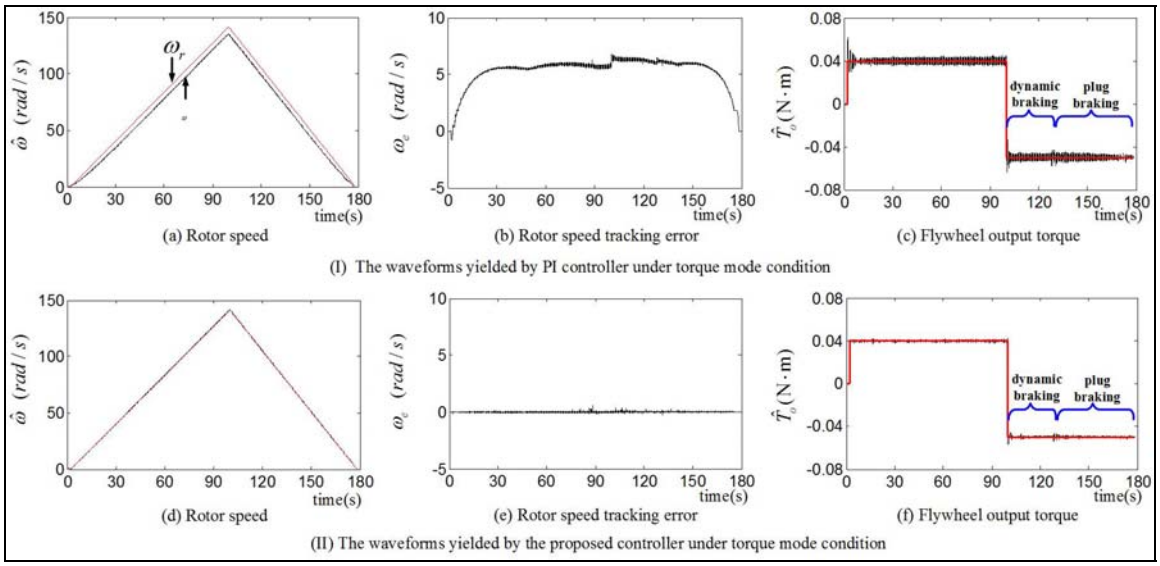

Fig. 9. Flywheel speed and torque waveforms during motoring and braking states under the speed mode condition.

performances are obviously improved.

V. Conclusion

The momentum flywheel is the key actuator for torque generation, and the parameter tuning of traditional linear controllers for the momentum flywheel, especially in braking operations, can be time-consuming and the tracking performance is limited. Some analyses and control methods are proposed in this paper to address these control issues of flywheel driving systems. At first, the singular perturbation theory is adopted to analyze the two-time scale quantities of flywheel dynamics and a high-precision torque controller is designed to cope with the inherited nonlinearity in braking dynamics. Meanwhile, a novel control strategy is introduced for plug braking. It shows a simple design process with superior control performance when compared with traditional distributed controllers. Finally, the effectiveness of the analysis and the superiority of the proposed MSFW torque control method have been verified by experiments.

Appendix

The flywheel motor dynamics during motoring operation can also be decomposed into a slow dynamic subsystem and a linearized fast dynamic subsystem, which can be represented as (31) and (32), respectively.

$$\begin{cases} 0 = D^s_{mt}(u_c + v_T) - v_T - v^s \\ 0 = v^s - R_{ab} i^s_m - k_e \omega \\ 0 = i^s_m + i^s \\ J\dfrac{d\omega}{dt} = -k_t i^s - B_d \omega - \tau_{dis} \end{cases} \tag{31}$$

$$\begin{cases} L_m \dfrac{di^e_m}{dt} = (u_c + v_T) d^e_{mt} - v^e \\ L_{ab} \dfrac{di^e}{dt} = -v^e + R_{ab} i^e_m \\ C_b \dfrac{dv^e}{dt} = i^e_m + i^e \end{cases} \tag{32}$$

From (31), the linear function mapping of i^s onto D^s_{mt} is given by:

$$\begin{cases} i^s = -i^s_m \\ \quad = f_{mt}(\omega, D^s_{mt}) = -(D^s_{mt}(u_c + v_T) - v_T - k_e\omega)/R_{ab} \\ v^s = D^s_{mt}(u_c + v_T) - v_T \end{cases} \tag{33}$$

According to (33), the linear function mapping onto Ds can be written as:

$$f^{-1}_{mt}(\omega, i^s) = (v_T - R_{ab} i^s + k_e\omega)/(u_c + v_T)$$

When the sliding surface for the fast subsystem is set as $\lambda_{mt}(i^e, v^e, i^e_m) = \lambda^1_{mt} i^e + \lambda^2_{mt} v^e + \lambda^3_{mt} i^e_m$, the composite controller output is given by:

$$D_{mt} = f^{-1}_{mt}(\omega, \hat{i}^s) + d^e_{mt} \tag{34}$$

where:

$$f^{-1}_{mt}(\omega, \hat{i}^s) = (v_T - R_{ab}\hat{i}^s + k_e\omega)/(u_c + v_T)$$

$$\hat{i}^s = (J\gamma_2 \int_t \omega_e + J\gamma_1 \omega_e - J\dot{\omega}_r - B_d\omega - \tau_{dis})/k_t$$

and:

$$d^e_{mt} = -L_m(\sigma\rho_{vs}(\lambda_{mt}) + k\lambda_{mt})/(\lambda^3_{mt} u_c + \lambda^3_{mt} v_T)$$

Acknowledgment

This work was supported by the National Natural Science Foundation of China under Grant 61403015, and SAST Fund 2016078.

REFERENCES

[1] D. Su and G. Liu, "The use of complex variables and frequency characteristics for stability analysis of magnetically suspended flywheels," *Proc IMechE, Part I: J Systems and Control Engineering*. Vol. 227, No. 9, pp. 674-685, Sep. 2013.

[2] W. Y. Zhou, D. Li, Q. Luo, and J. P. Jiang. "Design and test of a soft suspension system for cantilevered momentum wheel assembly," *Proc IMechE, Part G: J Aerospace Engineering,* Vol. 227, No. 7, pp. 1144-1160, Jun. 2013.

[3] C. Peng and J. C. Fang, "High-precision control for double-gimbal magnetically suspended control moment gyro via composite anti-disturbance control," *Proc IMechE, Part G: J Aerospace Engineering*, Vol. 229, No. 7, pp. 1183-1193, Aug. 2014.

[4] R. Varatharajoo, C. T. Wooi, and M. Mailah. "Attitude pointing enhancement for combined energy and attitude control system," *Acta Astronautica*, Vol. 68, pp. 2025-2028, Jun. 2011.

[5] X. X. Zhou, J. C. Fang, and G. Liu. "Precise braking torque control for attitude control flywheel with small inductance brushless DC motor," *IEEE Trans. Power Electron,* Vol. 28, No. 11, pp. 5380-5390, Nov. 2013.

[6] J. C. Fang, X. X. Zhou, and G. Liu, "Instantaneous torque control of small inductance brushless DC motor," *IEEE Trans. Power Electron*, Vol. 27, No. 12, pp. 4952-4964, Dec. 2012

[7] J. C. Fang, X. X. Zhou, and G. Liu. "Precise accelerated torque control for small inductance brushless DC motor," *IEEE Trans. Power Electron,* Vol. 28, No. 3, pp. 1400-1412, Nov. 2013.

[8] M. Conte, "Supercapacitors technical requirements for new applications," *Fuel Cells*, Vol. 10, No. 5, pp. 806-818, Dec. 2010.

[9] J. K. Ahn, K. H. Jung, D. H. Kim, H. B. Jin，H. S. Kim，and S. H. Hwang, "Analysis of a regenerative braking system for hybrid electric vehicles using an electro-mechanical brake," *Int. J. Automot. Technol.,* Vol. 10, No. 2, pp.229-234, Apr. 2009.

[10] H. Seki, K. Ishihara, and S. Tadakuma, "Novel regenerative braking control of electric power-assisted wheelchair for safety downhill road driving," *IEEE Trans. Ind. Electron*, Vol. 56, No. 5, pp.1393-1400, May. 2009.

[11] X. Nian, F. Peng, and H. Zhang, "Regenerative braking system of electric vehicle driven by brushless DC motor," *IEEE Trans. Ind. Electron*, Vol. 61, No. 10, pp. 5798-5808, Jan. 2014

[12] S. Vazquez, S. M. Lukic, E. Galvan, L. G. Franquelo, and J. M. Carrasco, "Energy storage systems for transport and grid applications," *IEEE Trans. Ind. Electron*, Vol. 57, No.12, pp.3881-3895, Dec. 2010

[13] O. C. Onar and A. Khaligh. "A novel integrated magnetic structure based DC/DC converter for hybrid battery/ultracapacitor energy storage systems*," IEEE Trans Smart Grid,* Vol. 3, No.1, pp. 296-307, Mar. 2012.

[14] R. Varatharajoo and S. Fasoulas. "The combined energy and attitude control system for small satellites — Earth observation missions," *Acta Astronautica*, Vol. 56, No.1, pp.251–259, Jan. 2005.

[15] P. V. Kokotović, "Applications of singular perturbation techniques to control problems," *SIAM review*, Vol. 26, No. 4, pp. 501-550, Jul. 1984.

[16] X. Zhang and Z. Lu. "A new BLDC motor drives method based on BUCK converter for torque ripple reduction," in *IEEE 5th International Conference on Power Electronics and Motion Control*, Vol. 3, pp. 1-4, 2006

[17] T. Lluís, D. B. Fernando, and G. B. Oriol, "Linear parameter-varying control of permanent magnet synchronous generators for wind power systems," *IET Power Electron,* Vol. 7, No. 3, pp. 692-704, Mar. 2014.

[18] Q. Chen, J. Jiang, S. Liu, and C. Zhang, "A novel sliding mode observer for state of charge estimation of EV lithium batteries," *Journal of Power Electronics*, Vol. 16, No. 3, pp. 1131-1140, May 2016.

[19] A. Abderrezak and K. Madjid, "Sensor fault detection, localization, and system reconfiguration with a sliding mode observer and adaptive threshold of PMSMs," *Journal of Power Electronics*, Vol. 16, No. 3, pp. 1012-1024, May 2016.

[20] H. Wang, S. Li, J. Yang, and X. P. Zhou "Continuous sliding mode control for permanent magnet synchronous motor speed regulation systems under time-varying disturbances," *Journal of Power Electronics*, Vol. 16, No. 4, pp. 1324-1335, Jul. 2016.

[21] Z. Wang, Y. Mao, Z. Hu, and Y. Xie "A sliding mode control design based on the reaching law for matrix rectifiers," *Journal of Power Electronics*, Vol. 16, No. 3, pp. 1122-1130, May 2016.

[22] A. E. Ahmed, H. M. Schwartz, and V. C. Aitken, "Sliding mode control for singularly perturbed system," in *5th Asian Control Conference IEEE*, Vol. 3, 2004.

Xinxiu Zhou received her B.S. degree from Yanshan University, Hebei, China, in 2006; and her Ph.D. degree from Beihang University, Beijing, China, in 2013. She is presently working as a Research Member of the Key Laboratory of Fundamental Science for National Defense, Novel Inertial Instrument and Navigation System Technology, Beihang University. Her current research interests include motor control, power electronics, and spacecraft attitude control.

Dan Su was born in August 1989. He received his B.S. degree from Hunan University, Changsha, China, in 2011; and his M.S. degree from Beihang University, Beijing, China, in 2014. He is presently working towards his Ph.D. degree at the City University of Hong Kong, Hong Kong SAR, China. His current research interests include the precise control of magnetic bearings, the high speed motor systems, computer vision and human-machine interface.